Crystal structure of importin-α3 bound to the nuclear localization signal of Ran-binding protein 3

Masako Koyama [a] **and Yoshiyuki Matsuura** [a,b,*]

[a]*Division of Biological Science, and* [b]*Structural Biology Research Center, Graduate School of Science, Nagoya University, Japan*.

* Corresponding author at: Division of Biological Science, Graduate School of Science, Nagoya University, Furo-cho, Chikusa-ku, Nagoya 464-8602, Japan.

E-mail: matsuura.yoshiyuki@d.mbox.nagoya-u.ac.jp

Abstract

Ran-binding protein 3 (RanBP3) is a primarily nuclear Ran-binding protein that functions as an accessory factor in the Ran GTPase system. RanBP3 associates with Ran-specific nucleotide exchange factor RCC1 and enhances its catalytic activity towards Ran. RanBP3 also promotes CRM1-mediated nuclear export as well as CRM1-independent nuclear export of β-catenin, Smad2, and Smad3. Nuclear import of RanBP3 is dependent on the nuclear import adaptor protein importin-α and, RanBP3 is imported more efficiently by importin-α3 than by other members of the importin-α family. Protein kinase signaling pathways control nucleocytoplasmic transport through phosphorylation of RanBP3 at Ser58, immediately C-terminal to the nuclear localization signal (NLS) in the N-terminal region of RanBP3. Here we report the crystal structure of human importin-α3 bound to an N-terminal fragment of human RanBP3 containing the NLS sequence that is necessary and sufficient for nuclear import. The structure reveals that RanBP3 binds to importin-α3 residues that are strictly conserved in all seven isoforms of human importin-α at the major NLS-binding site, indicating that the region of importin-α outside the NLS-binding site, possibly the autoinhibotory importin-β1-binding domain, may be the key determinant for the preferential binding of RanBP3 to importin-α3. Computational docking simulation indicates that phosphorylation of RanBP3 at Ser58 could potentially stabilize the association of RanBP3 with importin-α through interactions between the phosphate moiety of phospho-Ser58 of RanBP3 and a cluster of basic residues (Arg96 and Lys97 in importin-α3) on armadillo repeat 1 of importin-α.

Keywords: nuclear import; importin; NLS; RanBP3; phosphorylation

1. Introduction

Ran is a Ras-related small GTPase that is involved in diverse cellular processes, including nucleocytoplasmic transport, mitotic spindle assembly, and post-mitotic nuclear assembly (reviewed in [1]). Ran-binding protein 3 (RanBP3) is an accessory factor in the Ran GTPase system and belongs to a family of proteins that share a homologous Ran-GTP binding domain (RanBD) of about 120 amino acids [2]. N-terminal to the RanBD, RanBP3 has phenylalanine-glycine (FG)-repeat motifs, characteristic of a subgroup of nucleoporins localized at nuclear pore complexes [2]. Unlike nucleoporins, however, RanBP3 shows a diffuse intranuclear distribution excluding nucleoli in interphase cells [2]. RanBP3 associates with Ran-specific nucleotide exchange factor RCC1 and enhances its catalytic activity towards Ran [3]. RanBP3 accelerates formation of the CRM1 nuclear export complex [4] and promotes CRM1-mediated nuclear export [5,6]. RanBP3 also facilitates CRM1-independent nuclear export of β-catenin, Smad2, and Smad3, thereby negatively regulating Wnt signaling and TGF-β signaling [7,8].

Nuclear import of RanBP3 occurs via importin-α (Impα)-importin-β1 (Impβ1)-dependent pathway [9]. In this classical nuclear import pathway, the Impα adaptor proteins bind cargo proteins possessing the nuclear localization signal (NLS), and heterodimerize with Impβ1 through the N-terminal Impβ1-binding (IBB) domain, forming nuclear import complexes that carry cargo proteins from the cytoplasm to the nucleus through nuclear pore complexes (reviewed in [10,11]). The IBB domain of Impα has NLS-like sequence that inhibits the binding of NLS-containing cargo to the NLS-binding armadillo (ARM) repeat domain of Impα [12]. The association of Impβ1 with the IBB domain of Impα relieves the autoinhibition by the IBB domain, and thereby increases the affinity of NLS-cargo to Impα [13]. Human cells have seven

Impα isoforms (Impα1, Impα3, Impα4, Impα5, Impα6, Impα7, and Impα8), each of which has different substrate specificity (reviewed in [14,15]). It has been shown that RanBP3 is imported more efficiently by Impα3 than by other members of the Impα family [9].

The residues 40-57 of RanBP3 (the residue number refers to that of isoform 3, also known as RanBP3-b, which appears to be the primary transcript [9]) have been identified as the NLS sequence that is necessary and sufficient for nuclear import [9]. Welch *et al*. suggested that this is an "unusual" NLS that binds preferentially to Impα3 [9]. Interestingly, protein kinase signaling pathways (the PI3K/Akt and Ras/ERK/RSK pathways) control nucleocytoplasmic transport through phosphorylation of RanBP3 at Ser58, immediately C-terminal to the NLS, by unknown mechanisms [16-19]. In the present study, we report structural characterization of the interactions between the RanBP3 NLS and Impα3.

2. Materials and Methods

2.1 Preparation of ΔIBB Impα3-RanBP3 NLS complex for crystallization

N-terminally His_6- and S-tagged ΔIBB Impα3 (human, residues 70-485; UniProt code, O00629) and N-terminally GST-tagged RanBP3 NLS (human, isoform 3, also known as RanBP3-b, residues 31-60; UniProt code, Q9H6Z4) were expressed separately from pET30a-TEV [20] and pGEX-TEV [20], respectively, in the *E. coli* host strain BL21-CodonPlus(DE3)RIL (Stratagene). After harvesting, the two sets of cells were mixed, suspended in buffer A [30 mM Tris-HCl pH 7.5, 10 mM imidazole, 500 mM NaCl, 1 mM phenylmethylsulfonyl fluoride (PMSF), and 7 mM 2-mercaptoethanol] and lysed by sonication on ice. All subsequent steps were performed at 4°C. Clarified lysates were loaded onto Ni-NTA resin (Qiagen), washed with buffer A containing 25 mM imidazole, eluted with buffer A containing 150 mM imidazole and 0.05% Tween20. After incubating the Ni-NTA eluate with glutathione-Sepharose 4B resin (GE Healthcare) overnight and washing with buffer B (10 mM Tris-HCl pH 7.5, 150 mM NaCl, 2 mM 2-mercaptoethanol, and 0.05% Tween20), the GST- and His_6/S-tags were removed with His-TEV protease (0.01 mg/ml) in buffer B containing 0.2 mM 4-(2-aminoethyl) benzenesulfonyl fluoride hydrochloride (AEBSF). The ΔIBB Impα3-RanBP3 NLS complex released from the resin was finally purified over Superdex200 (GE Healthcare) in buffer C (10 mM Tris-HCl pH 7.5, 100 mM NaCl, and 2 mM 2-mercaptoethanol). The complex was concentrated to 10 mg/ml using a 3 kDa molecular weight cutoff Amicon Ultra centrifugal filter (Millipore).

2.2 Crystallization, data collection, and structure determination

Crystals of ΔIBB Impα3-RanBP3 NLS complex were obtained using hanging drop vapor diffusion method at 20 °C. The crystals were grown by mixing equal volumes (1.5 μl each) of the protein solution (10 mg/ml in buffer C) with the precipitant solution consisting of 0.1 M Tris-HCl pH 8.0 and 12% PEG8000. Crystals were serially transferred to 0.1 M Tris-HCl pH 8.0, 16% PEG8000, and 15% glycerol in three steps and flash-cooled in liquid nitrogen. X-ray diffraction datasets were collected at 95 K at the Photon Factory beamline BL-17A using an ADSC Quantum 315r CCD detector at a wavelength of 0.98 Å. Diffraction data were processed using iMOSFLM and CCP4 programs [21]. Crystals belonged to space group $P2_1$ with cell dimensions a = 47.97 Å, b = 60.22 Å, c = 85.02 Å, β = 100.54° and had one complex in the asymmetric unit. The intensities were highly anisotropic: diffraction data extended to 3.0 Å along a^* and b^* but not much beyond 3.4 Å along c^* (eigenvalue ratios of the anisotropic distribution of $|F|$ = 0.37, 0.54, 1.0). The structure was solved by molecular replacement using MOLREP [22] using the structure of ΔIBB Impα3 bound to influenza A virus PB2 (PDB code, 4UAE) [23] as a search model. The structures were refined by iterative cycles of model building using COOT [24] and refinement using PHENIX [25]. MolProbity [26] was used to validate the final model. Structural figures were produced using CCP4MG [27]. Coordinates and structure factors have been deposited in the PDB with accession code 5XZX.

2.3 Molecular docking

In silico docking of Ser58-phosphorylated RanBP3 NLS peptide (residues 46-59) to ΔIBB Impα3 was performed using the molecular docking program Autodock Vina [28]. Prior to docking, hydrogen atoms, Gasteiger partial charges, and ligand torsions were added using the program AutoDockTool in the MGLtools software [29]. The search space for docking was restricted in a cubic box of 40 Å × 40 Å × 40 Å

centered on the major NLS-binding site. The Impα3 structure was kept rigid during simulation. The most plausible model was selected according to the calculated binding affinity energy.

3. Results and Discussion

3.1 Crystal structure of Impα3 bound to non-phosphorylated NLS of RanBP3

To elucidate the mechanism of RanBP3 NLS recognition by Impα3, we grew crystals and solved the 3.0-Å-resolution structure of the NLS-binding ARM repeat domain of human Impα3 bound to human RanBP3 (residues 31-60, non-phosphorylated) (Fig. 1). The structure was refined to free and working *R*-factor values of 28.1% and 22.7%, respectively (Table 1). Residues 46-59 of RanBP3 bound to the major NLS-binding site in an extended conformation were identified unambiguously in the electron density map (Fig. 1A). The other residues of RanBP3 did not have defined electron density, indicating that these residues were disordered in the crystal.

In the crystal structure, residues 52-55 (^{52}KRER^{55}) of RanBP3 occupy the four principal binding cavities (the so-called P2-P5 positions; reviewed in [30]) at the major NLS-binding site, with flanking noncharged residues of RanBP3 making additional contributions to RanBP3-Impα3 association (Fig. 1B). Just upstream of the basic cluster (^{52}KRER^{55}), Cys48^{RanBP3} forms a hydrogen bond with Tyr268$^{Imp\alpha_3}$, and the aliphatic ring of Pro49^{RanBP3} contacts the nonpolar side chain of Trp264$^{Imp\alpha_3}$. Lys52^{RanBP3} at the P2 position forms a salt bridge with Asp187$^{Imp\alpha_3}$ and hydrogen bonds with Thr150$^{Imp\alpha_3}$ and main chain carbonyl group of Gly145$^{Imp\alpha_3}$. Arg53^{RanBP3} at the P3 position is sandwiched between Trp222$^{Imp\alpha_3}$ and Trp179$^{Imp\alpha_3}$ and forms a hydrogen bond with Asn219$^{Imp\alpha_3}$. The observation that Lys52^{RanBP3} and Arg53^{RanBP3} bind to the P2 and P3 acidic pockets at the major NLS-binding site is consistent with previous mutational analyses that showed that substitution of these basic residues with alanines abolish nuclear import [9]. Arg55^{RanBP3} at the P5 position is sandwiched between Trp179$^{Imp\alpha_3}$ and Trp137$^{Imp\alpha_3}$ and forms a hydrogen bond with Gln176$^{Imp\alpha_3}$. Arg55^{RanBP3} also makes a long-range electrostatic interaction with

Glu175^{Impα3}. C-terminal to the cluster of basic residues, Ser57^{RanBP3} makes hydrogen bonds with Ser100^{Impα3}. These interactions are supplemented with hydrogen bonds formed between the main chain of RanBP3 and Arg229^{Impα3}, Asn226^{Impα3}, Asn183^{Impα3}, Asn141^{Impα3}, and Trp137^{Impα3}.

Inspection of amino acid sequence alignment of the seven human Impα isoforms shows that the amino acid residues of Impα3 that directly contact the NLS residues of RanBP3 are strictly conserved (Fig. 2). This raises the question of why RanBP3 binds preferentially to Impα3 [9]. In this context, it is interesting to note that, although the Impα residues that form the NLS-binding site are highly conserved, the amino acid sequence outside the NLS-binding armadillo repeat domain is more divergent and, consequently, the autoinhibitory activity of the IBB domain differs between the Impα isoforms [31]. A previous semi-quantitative study using GST pull-down assay suggested that subtle differences in the IBB domain result in different levels of autoinhibition among Impα isoforms: Impα1 has the strongest autoinhibiton, Impα5 and Impα7 have looser autoinhibition, and Impα3 has the weakest autoinhibition [31]. It therefore seems likely that the diminished autoinhibition in Impα3 accounts for the preferential binding of RanBP3 to Impα3.

3.2 A possible structural model for the complex formed between Ser58-phosphorylated RanBP3 NLS and Impα3

In the light of the functional importance of the phosphorylation of Ser58 [16-19], immediately C-terminal to the NLS of RanBP3, an interesting feature of the crystal structure of the RanBP3-Impα3 complex is that the C-terminus of the NLS is located quite close to a cluster of basic residues (Arg96 and Lys97) on ARM repeat 1 of Impα3 (Fig. 1B). This indicates that, when Ser58 of RanBP3 is phosphorylated, the side

chain of phospho-Ser58 might make energetically favorable electrostatic interactions with these basic residues of Impα3, thereby providing additional stabilizing forces to the association of RanBP3 with Impα3. To explore this possibility, we performed computational docking simulation using Autodock tools [28,29]. The docking simulation proposed a possible structural model of the complex formed between Ser58-phosphorylated RanBP3 NLS and Impα3 (Fig. 3). In this structural model, the phosphate moiety of phosphor-Ser58^{RanBP3} makes bidentate salt bridges with Arg96$^{Imp\alpha_3}$ and also makes a long-range electrostatic interaction with Lys97$^{Imp\alpha_3}$ (Fig. 3). These basic residues are strictly conserved in all isoforms of human Impα (Fig. 2), and so the same interactions may enhance RanBP3 binding to all isoforms of human Impα. Although the validity of this model needs to be tested experimentally, this model indicates that phosphorylation-dependent interactions between RanBP3 and Impα may account for the observation that Akt activation promotes nuclear accumulation of Ser58-phosphorylated RanBP3 in cancer cells [19]. It may be worthwhile to investigate further whether the regulation of various RanBP3 functions through phosphorylation at Ser58 [16-19] is due to phosphorylation-dependent modulation of RanBP3-Impα interactions.

Conflict of interest

The authors have no conflict of interest to declare.

Acknowledgments

We thank Hidemi Hirano for technical assistance and discussion. We thank the staff of Photon Factory for assistance during X-ray diffraction data collection.

References

[1] M. Dasso, The Ran GTPase: theme and variations, Curr Biol 12 (2002) R502-508.

[2] L. Mueller, V.C. Cordes, F.R. Bischoff, H. Ponstingl, Human RanBP3, a group of nuclear RanGTP binding proteins, FEBS Lett 427 (1998) 330-336.

[3] M.E. Nemergut, M.E. Lindsay, A.M. Brownawell, I.G. Macara, Ran-binding protein 3 links Crm1 to the Ran guanine nucleotide exchange factor, J Biol Chem 277 (2002) 17385-17388.

[4] M. Koyama, N. Shirai, Y. Matsuura, Structural insights into how Yrb2p accelerates the assembly of the Xpo1p nuclear export complex, Cell Rep 9 (2014) 983-995.

[5] L. Englmeier, M. Fornerod, F.R. Bischoff, C. Petosa, I.W. Mattaj, U. Kutay, RanBP3 influences interactions between CRM1 and its nuclear protein export substrates, EMBO Rep 2 (2001) 926-932.

[6] M.E. Lindsay, J.M. Holaska, K. Welch, B.M. Paschal, I.G. Macara, Ran-binding protein 3 is a cofactor for Crm1-mediated nuclear protein export, J Cell Biol 153 (2001) 1391-1402.

[7] J. Hendriksen, F. Fagotto, H. van der Velde, M. van Schie, J. Noordermeer, M. Fornerod, RanBP3 enhances nuclear export of active (beta)-catenin independently of CRM1, J Cell Biol 171 (2005) 785-797.

[8] F. Dai, X. Lin, C. Chang, X.H. Feng, Nuclear export of Smad2 and Smad3 by RanBP3 facilitates termination of TGF-beta signaling, Dev Cell 16 (2009) 345-357.

[9] K. Welch, J. Franke, M. Kohler, I.G. Macara, RanBP3 contains an unusual nuclear localization signal that is imported preferentially by importin-alpha3, Mol Cell Biol 19 (1999) 8400-8411.

[10] D. Gorlich, U. Kutay, Transport between the cell nucleus and the cytoplasm, Annu Rev Cell Dev Biol 15 (1999) 607-660.

[11] M. Stewart, Molecular mechanism of the nuclear protein import cycle, Nat Rev Mol Cell Biol 8 (2007) 195-208.

[12] B. Kobe, Autoinhibition by an internal nuclear localization signal revealed by the crystal structure of mammalian importin alpha, Nat Struct Biol 6 (1999) 388-397.

[13] B. Catimel, T. Teh, M.R. Fontes, I.G. Jennings, D.A. Jans, G.J. Howlett, E.C. Nice, B. Kobe, Biophysical characterization of interactions involving importin-alpha during nuclear import, J Biol Chem 276 (2001) 34189-34198.

[14] R.A. Pumroy, G. Cingolani, Diversification of importin-alpha isoforms in cellular trafficking and disease states, Biochem J 466 (2015) 13-28.

[15] Y. Miyamoto, K. Yamada, Y. Yoneda, Importin alpha: a key molecule in nuclear transport and non-transport functions, J Biochem 160 (2016) 69-75.

[16] S.O. Yoon, S. Shin, Y. Liu, B.A. Ballif, M.S. Woo, S.P. Gygi, J. Blenis, Ran-binding protein 3 phosphorylation links the Ras and PI3-kinase pathways to nucleocytoplasmic transport, Mol Cell 29 (2008) 362-375.

[17] F. Dai, T. Shen, Z. Li, X. Lin, X.H. Feng, PPM1A dephosphorylates RanBP3 to enable efficient nuclear export of Smad2 and Smad3, EMBO Rep 12 (2011) 1175-1181.

[18] R. Predicala, Y. Zhou, The role of Ran-binding protein 3 during influenza A virus replication, J Gen Virol 94 (2013) 977-984.

[19] A. Lorenzato, M. Biolatti, G. Delogu, G. Capobianco, C. Farace, S. Dessole, A. Cossu, F. Tanda, R. Madeddu, M. Olivero, M.F. Di Renzo, AKT activation drives the nuclear localization of CSE1L and a pro-oncogenic transcriptional activation in ovarian cancer cells, Exp Cell Res 319 (2013) 2627-2636.

[20] Y. Matsuura, M. Stewart, Structural basis for the assembly of a nuclear export complex, Nature 432 (2004) 872-877.

[21] M.D. Winn, C.C. Ballard, K.D. Cowtan, E.J. Dodson, P. Emsley, P.R. Evans, R.M. Keegan, E.B. Krissinel, A.G. Leslie, A. McCoy, S.J. McNicholas, G.N. Murshudov, N.S. Pannu, E.A. Potterton, H.R. Powell, R.J. Read, A. Vagin, K.S. Wilson, Overview of the CCP4 suite and current developments, Acta Crystallogr D Biol Crystallogr 67 (2011) 235-242.

[22] A. Vagin, A. Teplyakov, MOLREP: an automated program for molecular replacement, J Appl Cryst 30 (1997) 1022-1025.

[23] R.A. Pumroy, S. Ke, D.J. Hart, U. Zachariae, G. Cingolani, Molecular determinants for nuclear import of influenza A PB2 by importin alpha isoforms 3 and 7, Structure 23 (2015) 374-384.

[24] P. Emsley, B. Lohkamp, W.G. Scott, K. Cowtan, Features and development of Coot, Acta Crystallogr D Biol Crystallogr 66 (2010) 486-501.

[25] P.D. Adams, P.V. Afonine, G. Bunkoczi, V.B. Chen, I.W. Davis, N. Echols, J.J. Headd, L.W. Hung, G.J. Kapral, R.W. Grosse-Kunstleve, A.J. McCoy, N.W. Moriarty, R. Oeffner, R.J. Read, D.C. Richardson, J.S. Richardson, T.C. Terwilliger, P.H. Zwart, PHENIX: a comprehensive Python-based system for macromolecular structure solution, Acta Crystallogr D Biol Crystallogr 66 (2010) 213-221.

[26] V.B. Chen, W.B. Arendall, 3rd, J.J. Headd, D.A. Keedy, R.M. Immormino, G.J. Kapral, L.W. Murray, J.S. Richardson, D.C. Richardson, MolProbity: all-atom structure validation for macromolecular crystallography, Acta Crystallogr D Biol Crystallogr 66 (2010) 12-21.

[27] S. McNicholas, E. Potterton, K.S. Wilson, M.E. Noble, Presenting your structures: the CCP4mg molecular-graphics software, Acta Crystallogr D Biol Crystallogr 67 (2011) 386-394.

[28] O. Trott, A.J. Olson, AutoDock Vina: improving the speed and accuracy of docking with a new scoring function, efficient optimization, and multithreading, J Comput Chem 31 (2010) 455-461.

[29] G.M. Morris, R. Huey, W. Lindstrom, M.F. Sanner, R.K. Belew, D.S. Goodsell, A.J. Olson, AutoDock4 and AutoDockTools4: Automated docking with selective receptor flexibility, J Comput Chem 30 (2009) 2785-2791.

[30] M. Christie, C.W. Chang, G. Rona, K.M. Smith, A.G. Stewart, A.A. Takeda, M.R. Fontes, M. Stewart, B.G. Vertessy, J.K. Forwood, B. Kobe, Structural Biology and Regulation of Protein Import into the Nucleus, J Mol Biol 428 (2016) 2060-2090.

[31] R.A. Pumroy, S. Ke, D.J. Hart, U. Zachariae, G. Cingolani, Molecular determinants for nuclear import of influenza A PB2 by importin alpha isoforms 3 and 7, Structure 23 (2015) 374-384.

[32] J.D. Thompson, D.G. Higgins, T.J. Gibson, CLUSTAL W: improving the sensitivity of progressive multiple sequence alignment through sequence weighting, position-specific gap penalties and weight matrix choice, Nucleic Acids Res 22 (1994) 4673-4680.

[33] A.M. Waterhouse, J.B. Procter, D.M. Martin, M. Clamp, G.J. Barton, Jalview Version 2--a multiple sequence alignment editor and analysis workbench, Bioinformatics 25 (2009) 1189-1191.

Figure legends

Fig. 1. Crystal structure of Impα3 bound to non-phosphorylated NLS of RanBP3. (A) Overall structure of ΔIBB Impα3 (ribbon representation) bound to RanBP3 NLS (stick representation). The omit F_o–F_c electron density map covering RanBP3 NLS is shown in blue mesh (contoured at 2.3σ). (B) A stereo view of the interactions between Impα3 (ribbon representation in light blue) and RanBP3 NLS (stick representation with green carbons) at the major NLS-binding site. Dashed lines represent hydrogen bonds, salt bridges, or electrostatic interactions.

Fig. 2. Amino acid sequence alignment of the seven isoforms of human Impα at the major NLS-binding site. The UniProt codes are: Impα1, P52292; Impα3, O00629; Impα4, O00505; Impα5, P52294; Impα6, O15131; Impα7, O60684; Impα8, A9QM74. Conserved residues are shaded. Asterisks above the sequence alignment denote the residues that directly contact RanBP3 in the crystal structure of Impα3-RanBP3 NLS complex. Arrows denote a conserved cluster of basic residues (Arg96 and Lys97 in Impα3) on ARM repeat 1. Sequences were aligned using ClustalW [32], and its output was visualized with the program Jalview [33].

Fig. 3. A structural model of a complex formed between Impα3 and Ser58-phosphorylated NLS of RanBP3. (A) Interactions between Impα3 (ribbon representation) and RanBP3 (stick representation with green carbons). Dashed lines represent hydrogen bonds, salt bridges, or electrostatic interactions. (B) Molecular surface of Impα3 at the major NLS-binding site colored according to electrostatic potential, shaded from blue (potential +150 mV) through white (potential 0 mV) to red (potential −150 mV). Orientation is the same as in (A).

Table 1. Crystallographic statistics.

Data collection	
Space group	$P2_1$
Unit cell dimensions	
a, *b*, *c* (Å)	47.97, 60.22, 85.02
α, β, γ (degree)	90, 100.54, 90
Wavelength (Å)	0.98
X-ray source	Photon Factory BL-17A
Resolution range (Å)[a]	48.86-3.00 (3.18-3.00)
No. of measured reflections[a]	33080 (5477)
No. of unique reflections[a]	9597 (1546)
Completeness (%)[a]	99.1 (99.6)
R_{merge} (%)[a]	5.3 (26.8)
Mean $I/\sigma(I)$[a]	12.0 (3.4)
Mean *I* half-set correlation CC(1/2)[a]	0.998 (0.977)
Multiplicity[a]	3.4 (3.5)
Refinement	
Resolution range (Å)[a]	37.13-3.00 (3.43-3.00)
R_{work} (%)[a]	22.7 (29.9)
R_{free} (%)[a]	28.1 (30.6)
No. of atoms	3304
No. of amino acids	428
Mean *B* factor (Å^2)	
Impα3	101.4
RanBP3	92.0
RMSD from ideality	
Bond lengths (Å)	0.002
Bond angles (degree)	0.502
Protein geometry[b]	
Rotamer outliers (%)	0
Ramachandran favored (%)	96.70
Ramachandran outliers (%)	0
Cβ deviations > 0.25 Å (%)	0
MolProbity score (percentile)	1.48 (100)
PDB code	5XZX

[a] Values in parentheses are for the highest-resolution shell.

[b] MolProbity was used to analyze the structure.

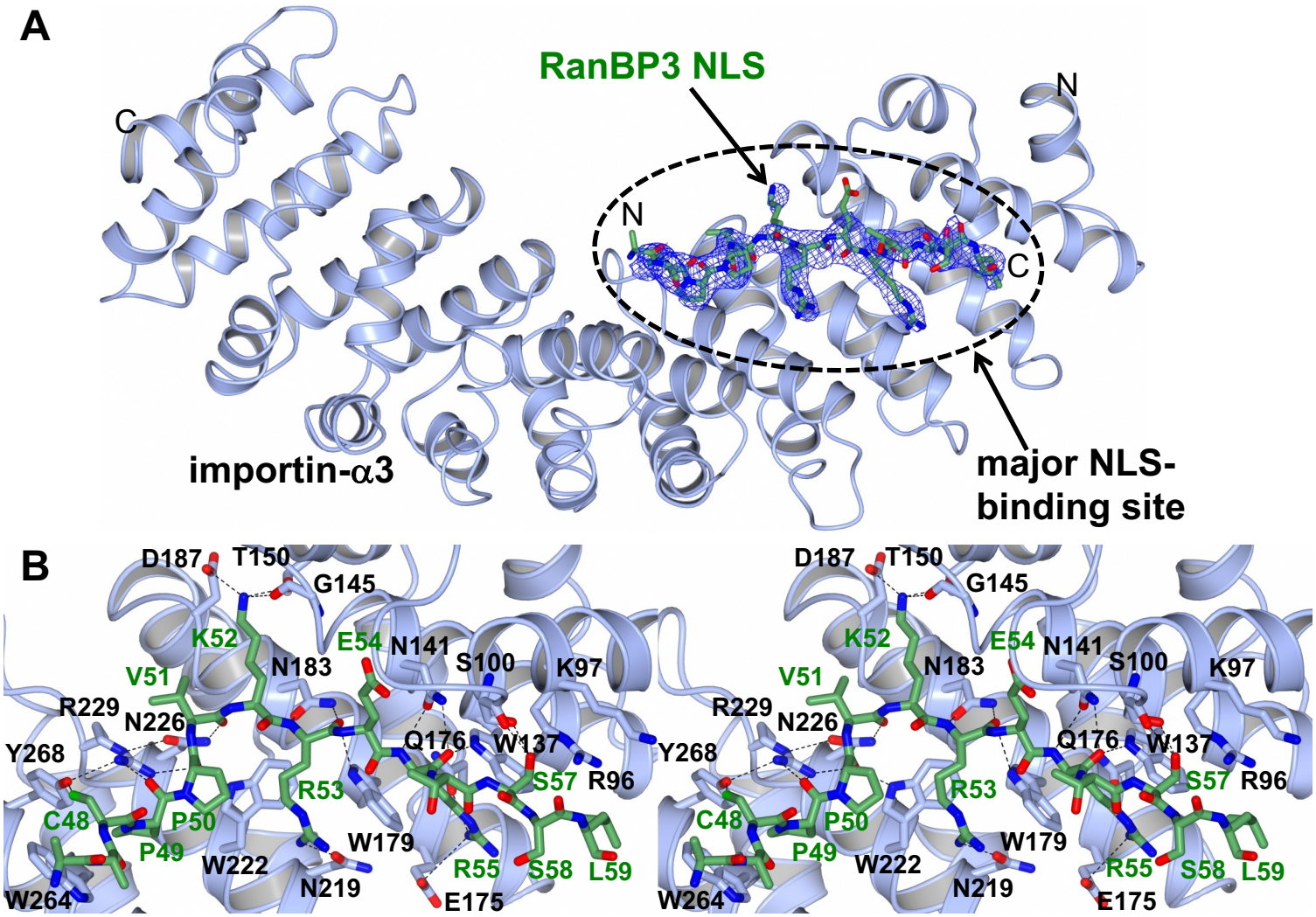
A
RanBP3 NLS
C
N
N
C
importin-α3
major NLS-
binding site
B
D187
T150
G145
K52
E54
N141
S100
K97
V51
N183
R229
N226
Y268
Q176
W137
S57
R96
R53
C48
P50
P49
W222
W179
R55
S58
L59
W264
N219
E175

Figure 1

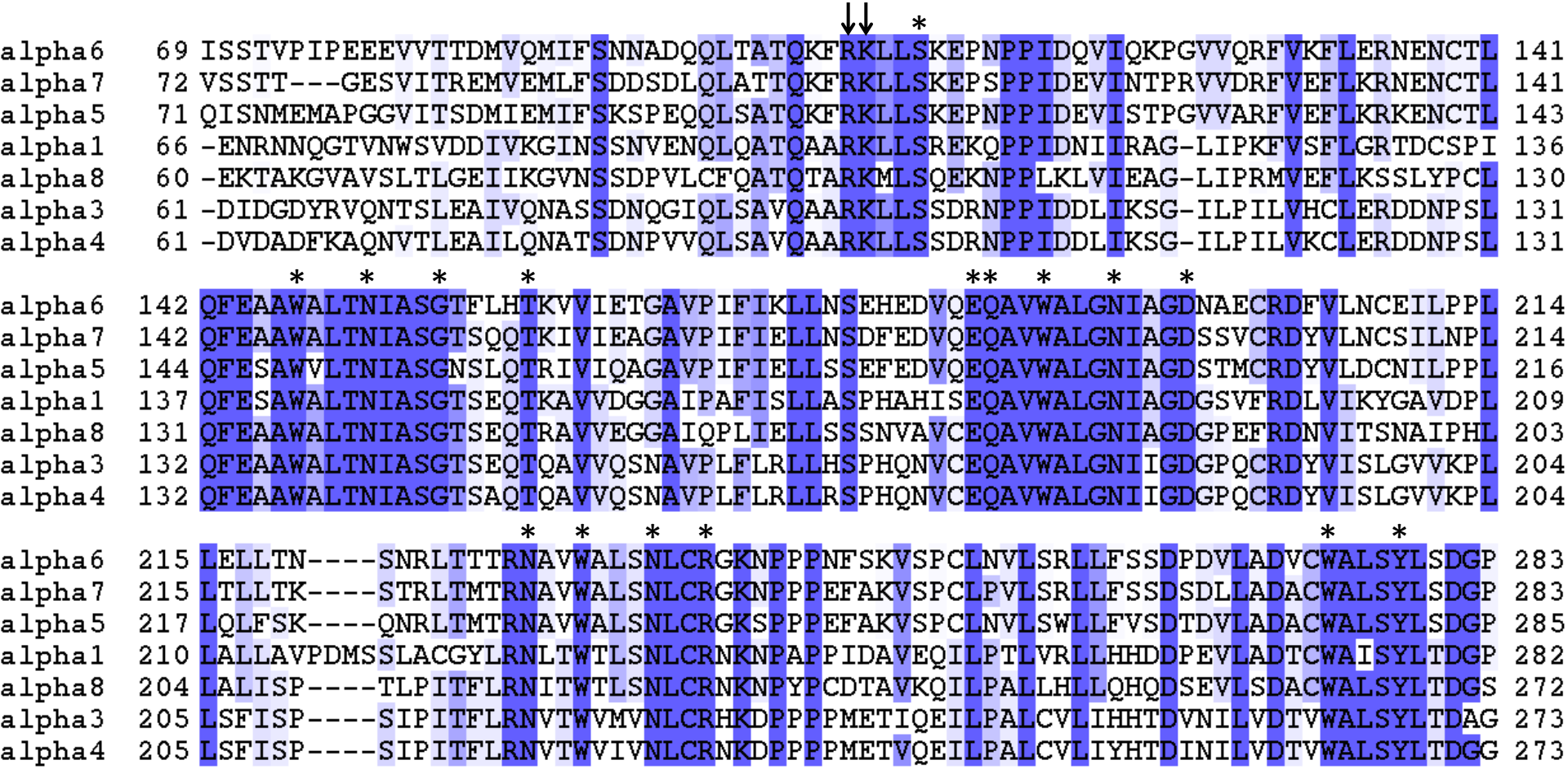
alpha6 69 ISSTVPIPEEEVVTTDMVQMIFSNNADQQLTATQKFRKLLSKEPNPPIDQVIQKPGVVQRFVKFLERNENCTL 141
alpha7 72 VSSTT---GESVITREMVEMLFSDDSDLQLATTQKFRKLLSKEPSPPIDEVINTPRVVDRFVEFLKRNENCTL 141
alpha5 71 QISNMEMAPGGVITSDMIEMIFSKSPEQQLSATQKFRKLLSKEPNPPIDEVISTPGVVARFVEFLKRKENCTL 143
alpha1 66 -ENRNNQGTVNWSVDDIVKGINSSNVENQLQATQAARKLLSREKQPPIDNIIRAG-LIPKFVSFLGRTDCSPI 136
alpha8 60 -EKTAKGVAVSLTLGEIIKGVNSSDPVLCFQATQTARKMLSQEKNPPLKLVIEAG-LIPRMVEFLKSSLYPCL 130
alpha3 61 -DIDGDYRVQNTSLEAIVQNASSDNQGIQLSAVQAARKLLSSDRNPPIDDLIKSG-ILPILVHCLERDDNPSL 131
alpha4 61 -DVDADFKAQNVTLEAILQNATSDNPVVQLSAVQAARKLLSSDRNPPIDDLIKSG-ILPILVKCLERDDNPSL 131
alpha6 142 QFEAAWALTNIASGTFLHTKVVIETGAVPIFIKLLNSEHEDVQEQAVWALGNIAGDNAECRDFVLNCEILPPL 214
alpha7 142 QFEAAWALTNIASGTSQQTKIVIEAGAVPIFIELLNSDFEDVQEQAVWALGNIAGDSSVCRDYVLNCSILNPL 214
alpha5 144 QFESAWVLTNIASGNSLQTRIVIQAGAVPIFIELLSSEFEDVQEQAVWALGNIAGDSTMCRDYVLDCNILPPL 216
alpha1 137 QFESAWALTNIASGTSEQTKAVVDGGAIPAFISLLASPHAHISEQAVWALGNIAGDGSVFRDLVIKYGAVDPL 209
alpha8 131 QFEAAWALTNIASGTSEQTRAVVEGGAIQPLIELLSSSNVAVCEQAVWALGNIAGDGPEFRDNVITSNAIPHL 203
alpha3 132 QFEAAWALTNIASGTSEQTQAVVQSNAVPLFLRLLHSPHQNVCEQAVWALGNIIGDGPQCRDYVISLGVVKPL 204
alpha4 132 QFEAAWALTNIASGTSAQTQAVVQSNAVPLFLRLLRSPHQNVCEQAVWALGNIIGDGPQCRDYVISLGVVKPL 204
alpha6 215 LELLTN----SNRLTTTRNAVWALSNLCRGKNPPPNFSKVSPCLNVLSRLLFSSDPDVLADVCWALSYLSDGP 283
alpha7 215 LTLLTK----STRLTMTRNAVWALSNLCRGKNPPPEFAKVSPCLPVLSRLLFSSDSDLLADACWALSYLSDGP 283
alpha5 217 LQLFSK----QNRLTMTRNAVWALSNLCRGKSPPPEFAKVSPCLNVLSWLLFVSDTDVLADACWALSYLSDGP 285
alpha1 210 LALLAVPDMSSLACGYLRNLTWTLSNLCRNKNPAPPIDAVEQILPTLVRLLHHDDPEVLADTCWAISYLTDGP 282
alpha8 204 LALISP----TLPITFLRNITWTLSNLCRNKNPYPCDTAVKQILPALLHLLQHQDSEVLSDACWALSYLTDGS 272
alpha3 205 LSFISP----SIPITFLRNVTWVMVNLCRHKDPPPPMETIQEILPALCVLIHHTDVNILVDTVWALSYLTDAG 273
alpha4 205 LSFISP----SIPITFLRNVTWVIVNLCRNKDPPPPMETVQEILPALCVLIYHTDINILVDTVWALSYLTDGG 273

Figure 2

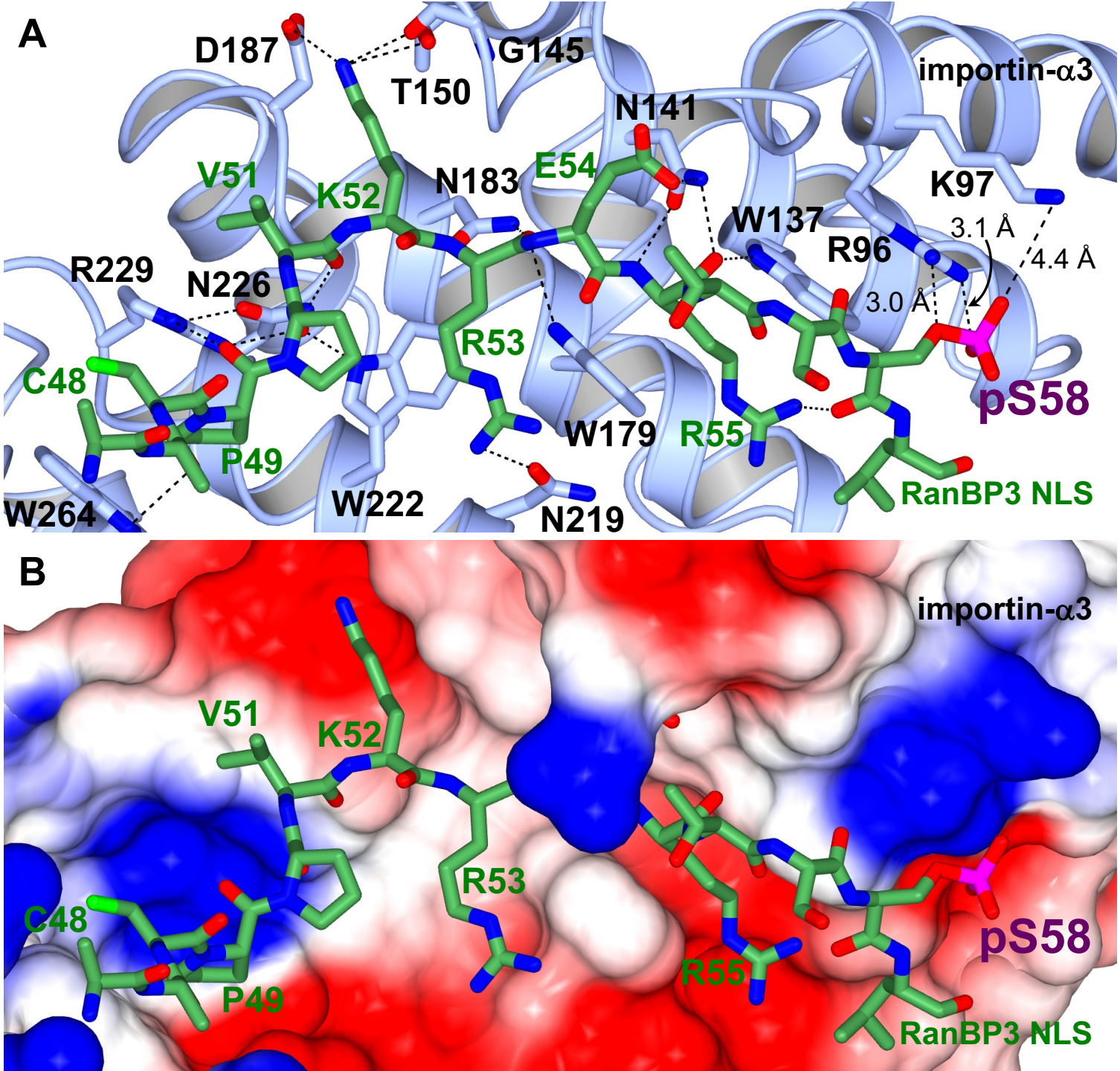
A
D187
T150
G145
importin-α3
N141
V51
K52
N183
E54
K97
W137
3.1 Å
R96
4.4 Å
3.0 Å
R229
N226
R53
C48
pS58
W179
R55
P49
RanBP3 NLS
W264
W222
N219
B
importin-α3
V51
K52
R53
C48
pS58
R55
P49
RanBP3 NLS

Figure 3